# Field-dependent Brownian relaxation dynamics of a superparamagnetic clustered-particle suspension

S. B. Trisnanto and Y. Kitamoto*

*Department of Innovative and Engineered Materials, Tokyo Institute of Technology, 4259 Nagatsuta, Midori-ku, Yokohama 226-8502, Japan*

(Received 14 April 2014; published 22 September 2014)

The distinguishable Brownian relaxation dynamics of a clustered-particle system of superparamagnetic iron oxide nanoparticle suspension compared to that of a dispersed-particle system has been experimentally investigated through characterization of the frequency and field strength dependences of complex magnetic susceptibility. We confirmed that the application of low sinusoidal magnetic field strength enables cluster rotation instead of individual particle rotations. Furthermore, we found that the cluster rotation was altered to individual particle rotations in higher field strength, resulting in a shorter Brownian relaxation time, which suggests a change in the hydrodynamic volume. This evolutional relaxation behavior was associated with a change in the fitting parameter which satisfies the empirical model of relaxation and further represents the significance of interparticle interactions in defining the nonlinearity of the magnetization response.

DOI: 10.1103/PhysRevE.90.032306 PACS number(s): 83.80.Hj, 75.75.Jn

## I. INTRODUCTION

Monodomain ferromagnetic nanoparticle suspension, with its physicochemical phenomenon of superparamagnetism, has been leading to many promising applications in the biomedical field [1–4]. The utilization of heat dissipation induced by relaxation losses of magnetic nanoparticles under an alternating magnetic field to kill cancer (magnetic hyperthermia) [5], the interpretation of nonlinear magnetization of magnetic particles as harmonic responses to develop an imaging system (magnetic particle imaging, MPI) [6], and the characterization of distinguishable relaxation times between bound and unbound magnetic nanoparticles to detect biological targets (magnetic immunoassay) [7] are currently of great interest. A remaining challenge has been to develop these sinusoidal magnetic-field-based applications with more biocompatible magnetic nanoparticles such as iron oxides [8]. Basically, the application of a sinusoidal magnetic field to superparamagnetic suspension will trigger two possible relaxation behaviors of the suspended particles. Brownian relaxation, which involves physical rotation, occurs when magnetic moment is locked in an easy axis of magnetization and the external magnetic force is greater than the rotational friction force of the particle. Otherwise, Neel relaxation employs the rotation of magnetic moment within particles by overcoming the anisotropy energy barrier. The mathematical formulations which explain how fast these phenomena take place can be found in [9] and [10]. The competing mechanism between both relaxations determines the magnetic susceptibility of the suspension.

Multivariable-dependent complex magnetic susceptibility is a decisive parameter in defining the heating efficiency of magnetic hyperthermia, image resolution of MPI, and detection sensitivity of magnetic immunoassay [11–13]. The relaxation dynamics of magnetic nanoparticles which specifies this parameter has been well studied through theoretical assessments [14–17], emphasizing that interparticle interactions appearing from such polydispersity should be carefully taken into account. Nevertheless, here, the term *relaxation dynamics* is limitedly addressed to dispersed particles and their Gaussian-like nonuniform size distribution in either the primary particle size corresponding to the crystallite size or the secondary particle size (hydrodynamic size), referring to the effective size in the liquid environment including aggregations. There is insufficient understanding of the dynamic behavior of such initially clustered particles (a group of particles interconnected by strong dipolar interaction within a hydrodynamic size) and its dependence on field strength.

The clustered particles, however, may originally exist in a stable superparamagnetic suspension instead of a time-dependent particle aggregation, a stochastic clustering process that mostly occurs in a polydispersive suspension owing to interparticle interactions [18,19], since the polymer coating should be able to prevent this and further improve dispersibility by providing steric stabilization [20,21]. The dynamic behavior of the clustered-particle system in the presence of a sinusoidal magnetic field should depend on the field strength; thus, it might be different from what was generally assessed in [15] in terms of the magnetization response. Therefore, we performed measurements of the complex magnetic susceptibility of superparamagnetic clustered-particle suspension compared with that of a dispersed-particle system to better understand their differences. In this paper, we further discuss the contribution of interparticle interactions specific to Brownian relaxation dynamics with a physical model of relaxation.

## II. EXPERIMENT

Concerning the linear response of relaxation, one may find that the delay in the magnetization response corresponds to $\tan^{-1}\omega\tau$ [22]. When an oscillating magnetic field with radian frequency $\omega$ is applied to magnetic nanoparticles, both Brownian and Neel relaxations may occur. But for each individual particle, only the dominant relaxation mechanism will be considered to determine the size-dependent effective relaxation time $\tau$ of the particles. This physical term contributes to defining the frequency response of the magnetization, which is mainly expressed as a complex form

*kitamoto.y.aa@m.titech.ac.jp

 

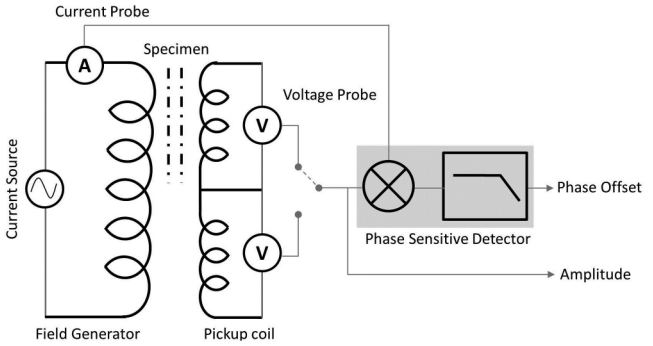


FIG. 1. Schematic diagram of the complex magnetic susceptibility measurement which includes a wave generator as the current source, a coil system for magnetic field generation and sensing, and a computerized-signal processing unit to measure signal parameters.

of magnetic susceptibility, $\chi(\omega) = \chi'(\omega) - i\chi''(\omega)$. These spectral responses of the real part $\chi'$ and the imaginary part $\chi''$ of magnetic susceptibility [5] allow us to study the relaxation phenomena of magnetic nanoparticles under an alternating magnetic field. Therefore, we carried out complex magnetization measurements in which the complex magnetic susceptibility itself was defined from the signal parameters of electromotive force generated by a pickup coil with and without magnetic nanoparticles. A simplified measurement diagram of our system is shown in Fig. 1. The presence of a specimen will slightly increase the amplitude of the output signal and shift the phase due to superposition between the magnetic field and magnetization. We then extracted these changes to estimate the real part and the imaginary part of the magnetic susceptibility.

The relaxation behaviors of magnetic nanoparticles in superparamagnetic suspension do not seem to be simple since not only the physical properties such as size but also considerable interparticle interactions define them. To further understand this phenomenon, especially at low frequency with regard to Brownian relaxation, we used two water-based superparamagnetic suspensions containing sodium $\alpha$-olefin sulfonate–coated iron oxide nanoparticles (specimen 1) and carboxydextran-coated iron oxide nanoparticles (specimen 2) in our experiment. A summary of the properties of the specimens is given in Table I. The actual particle diameter $D_m$ estimated from transmission electron microscopy (TEM) and the hydrodynamic diameter $D_h$ measured by a nanoparticle analyzer using dynamic light scattering (DLS; SZ-100 nanopartica, Horiba) are shown in Fig. 2. With regard to these properties, we categorized specimen 1 as a dispersed-particle system and and specimen 2 as a clustered-particle system (see Fig. 3). It was also expected that specimen 1 would

TABLE I. Physical properties of specimens.

| Specimen | Coating | $M_s$ (emu mL$^{-1}$) | $D_m$ (nm) | $D_h$ (nm) | $\rho$ (g mL$^{-1}$) |
|---|---|---|---|---|---|
| 1 | Sodium $\alpha$-olefin sulfonate | 30.70 | 10-20 | ~50 | 1.41 |
| 2 | Carboxydextran | 3.93 | ~7 | ~65 | 1.054 |

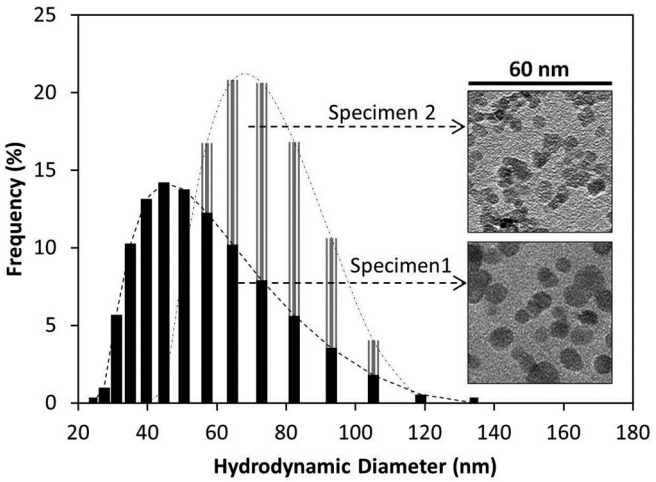


FIG. 2. The DLS measurement and TEM image of specimens (inset) show the nonuniformity of the corresponding hydrodynamic size and iron oxide particle size distribution.

show a shorter Brownian relaxation time and longer Neel relaxation time compared to specimen 2. We performed complex magnetic susceptibility measurements of relatively dense suspensions with a 40-$\mu$L specimen volume (equal to 56.38 mg of specimen 1 and 40.16 mg of specimen 2; from there we estimated the density of the specimens) under 6.5 and 65 Oe rms of sinusoidal magnetic field with various frequencies from 100 Hz to 2 MHz at room temperature. We also measured the field-strength-dependent magnetic susceptibility up to 65 Oe rms at 300 Hz and 300 kHz. Additional measurements of the magnetization responses of the specimens were done to define the saturation magnetization $M_s$ under 90 kOe of static field at 300 K and the temperature-dependent complex magnetic susceptibility using the Physical Properties Measurement System (PPMS, Quantum Design Inc.).

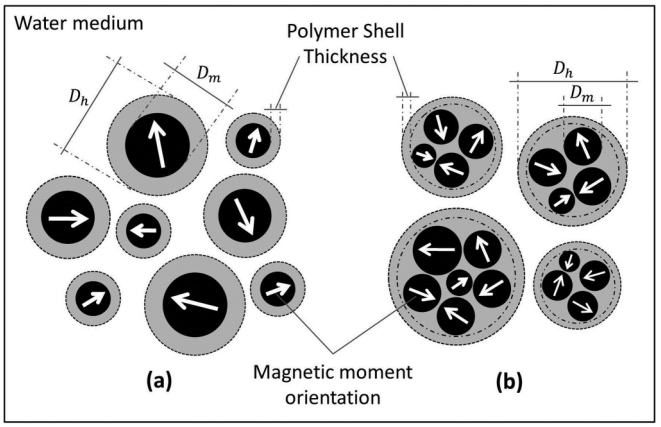


FIG. 3. Illustration of (a) a dispersed-particle system and (b) a clustered-particle system that may exist in water-based suspensions due to polymeric surface modification (gray) of iron oxide nanoparticles (black). White arrows show the orientation of the magnetic moment.

## III. RESULT

### A. Frequency- and field-strength-dependent magnetic susceptibility

In magnetic suspensions, several interactions lead to aggregation of magnetic nanoparticles at steady state, such as dipolar interaction or van der Waals interaction [15]. The application of low oscillatory magnetic field is possible to dominate those weakly attractive interactions so that the magnetized particles which experience field-strength-dependent magnetic torque can physically rotate. This means that the fragmentation induced by physical rotation is preferable to the aggregation of particles. Hence, it will enhance Brownian relaxation of particles. The measurement results of the imaginary part of the complex magnetic susceptibility depicted in Fig. 4 show the same feature by distinguishing a clear Brownian peak at around 1 kHz for specimen 1 and around 900 Hz for specimen 2 under 6.5 Oe of magnetic field strength. As shown in Fig. 4, for a constant applied magnetic field strength, the peak of the imaginary part of the magnetic susceptibility observed at the low-frequency response of magnetization could be attributed to the dominance of Brownian relaxation (the so-called Brownian peak), and at the higher frequency, it was attributed to Neel relaxations (the so-called Neel peak).

Nonlinear magnetization could clearly be observed as a decrease in the real part of the magnetic susceptibility at lower

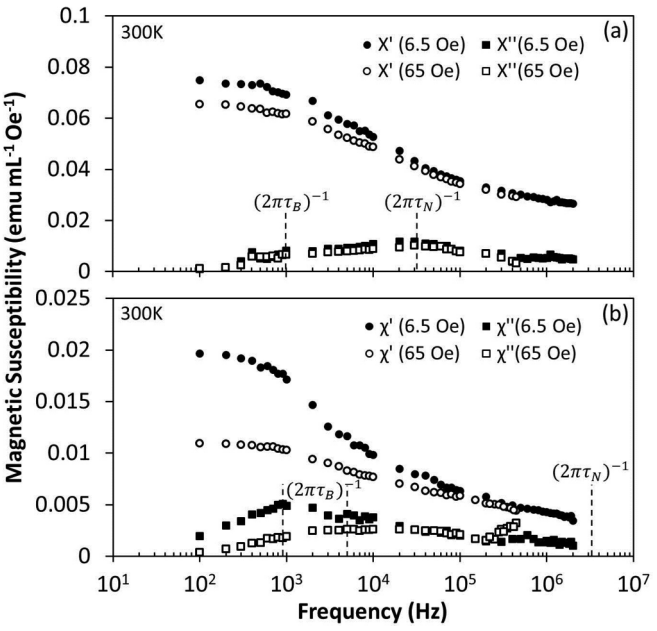


FIG. 4. The frequency-dependent complex magnetic susceptibility of (a) specimen 1 and (b) specimen 2 shows different trends in higher field strength and lower frequency due to the existing interparticle interactions. In specimen 1, the suspended particles are supposed to be individually dispersed so that the resulting dipolar interactions are much lower than those of specimen 2. The real part of the magnetic susceptibility under 6.5 Oe rms (solid circles) is generally larger than that under 65 Oe rms (open circles), while the imaginary part of the magnetic susceptibility under 6.5 Oe rms (solid squares) shows different peak positions compared to that under 65 Oe rms (open squares).

frequency in which Brownian relaxation was dominant. The dominance was further proven by the significant difference in magnetization responses in the solid phase (frozen state) and the liquid phase of the suspensions, as described in Figs. 5(a) and 5(b). At low temperature, particles were completely restrained from physically moving so that the magnetization responses were only because of Neel relaxation. However, at room temperature, the suspended particles were able to rotate freely under the application of an alternating magnetic field. Consequently, magnetization was strongly enhanced. This was found to be a discontinued pattern of temperature-dependent magnetic susceptibility. Another measurement of mean magnetization, $|M| = H\sqrt{(\chi')^2 - (i\chi'')^2}$, shown in Figs. 5(c) and 5(d), also states that the varying significance of interparticle interactions (dipolar magnetism) in each specimen can be associated with the apparent phenomenon of nonlinear magnetization [23].

Meanwhile, Zeeman energy may overcome the anisotropy energy of particles at higher magnetic field so that the probability to perform Neel relaxation increases. In Fig. 4, the Neel peak of specimen 1 can be observed at around 30 kHz. In the case of specimen 2, it cannot be confirmed because of the measurement limitation. However, due to the primary particle size, it can be approximated to be 3.58 MHz considering that the anisotropy constant of $Fe_3O_4$ is $3 \times 10^{-4}$ Jm$^{-3}$ [24]. At 65 Oe, the Neel relaxation in specimen 2 started to appear at a frequency above 300 kHz, which could not be seen at 6.5 Oe of applied field strength. Moreover, the Brownian peak was shifted from 900 Hz at 6.5 Oe to ~5 kHz at 65 Oe.

### B. Relaxation symmetry

To elucidate further the relaxation dynamics of superparamagnetic nanoparticles under an alternating magnetic field, it is worth understanding the relaxation time distribution. Polydispersive suspension is not likely to have a single relaxation time but multiple relaxation times [15]. The broadening distribution of the imaginary part of the magnetic susceptibility against the frequency observed in Fig. 4 indicates the contribution of polydispersity in defining the effective relaxation time. The empirical descriptions that are most frequently used to analyze the distribution of the relaxation time are the Cole-Cole symmetric model of relaxation [25], which introduces the $\alpha$ parameter as in Eq. (1), and the Cole-Davidson asymmetric model of relaxation [26], which introduces the $\beta$ parameter as in Eq. (2), where $\chi_s$ and $\chi_\infty$ are the limiting low- and high-frequency magnetic susceptibilities, respectively. The multiple relaxation times can be associated with the nonlinearity of $\chi''(\chi')/\omega$ or $\omega\chi''(\chi')$ curves with respect to Debye model allowing a single relaxation time [27],

$$\chi(\omega) = \chi_\infty + \frac{\chi_s - \chi_\infty}{1 + (i\omega\tau)^{1-\alpha}}, \tag{1}$$

$$\chi(\omega) = \chi_\infty + \frac{\chi_s - \chi_\infty}{(1 + i\omega\tau)^{\beta}}. \tag{2}$$

The imaginary part as a function of the real part of the Cole-Cole model and the Cole-Davidson model can be approximated by applying Eqs. (3) and (4). Using the experimental data in Fig. 4, we plotted $\chi''(\chi')$. The result

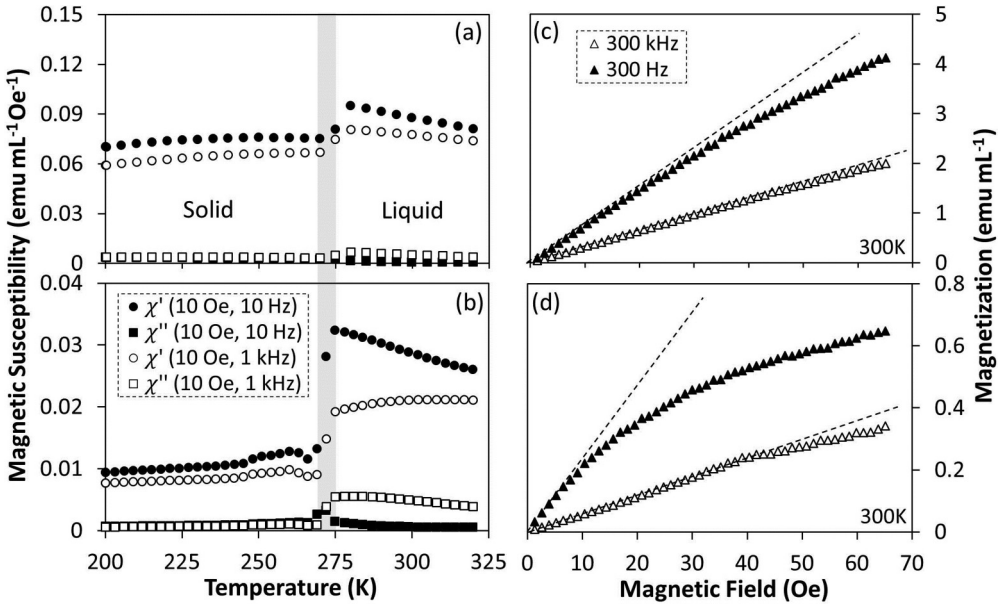


FIG. 5. The temperature- and field-strength-dependent complex magnetic susceptibilities of (a) and (c) specimen 1 and (b) and (d) specimen 2 indicate the dominant contribution of Brownian relaxation to the nonlinear response of magnetization. High temperature, at which the phase transition from solid to liquid occurs, induces a considerable increase in magnetic susceptibility. In the liquid state, the real part of the magnetic susceptibility at 10 Hz (solid circles) is higher than 1 kHz (open circles), whereas the imaginary part of the magnetic susceptibility at 10 Hz (solid squares) and 1 kHz (open squares) shows the opposite trend, indicating higher relaxation loss. The magnetization responses of both specimens show high nonlinearity at 300 Hz (solid triangles) but are further linearized at 300 kHz (open triangles).

was then compared with a suitable numerical simulation of these equations:

$$\chi'' = (\chi' - \chi_\infty)\frac{(\omega\tau)^{(1-\alpha)}\cos\frac{1}{2}\alpha\pi}{1+(\omega\tau)^{(1-\alpha)}\sin\frac{1}{2}\alpha\pi}, \quad (3)$$

$$\chi'' = (\chi' - \chi_\infty)\tan(\beta\tan^{-1}\omega\tau). \quad (4)$$

According to Fig. 6(a), $\chi''(\chi')$ plots of specimen 1 were compatible with the Cole-Cole model, which means that only relaxation of individual particles occurs. From Fig. 6(a), the initial Brownian relaxation region, which is limited by $\chi_s = 0.076$ emu mL$^{-1}$ Oe$^{-1}$ and $\chi_\infty = 0.055$ emu mL$^{-1}$ Oe$^{-1}$, and the initial Neel region, which is limited by $\chi_s = 0.070$ emu mL$^{-1}$ Oe$^{-1}$ and $\chi_\infty = 0.024$ emu mL$^{-1}$ Oe$^{-1}$, were identified. Actually, when a low-frequency magnetic field is applied, single dispersed particles may experience large enough magnetic torque to physically rotate themselves along their hydrodynamic axis. For constant field strength, increasing frequency should increase the energy absorption due to a larger phase lag of the induced magnetization when the frequency of the applied field is lower than the relaxation frequency. Otherwise, magnetization responses cannot follow the oscillation of magnetic field if the applied frequency far exceeds the relaxation frequency. These create the symmetric curve of the $\chi''(\chi')$ projection. In addition, as frequency increases, particle rotation is inhibited by the increase of the rotational friction forces leading to immobilization, so that only rotations of the magnetic moment will remain working. Thus, the change in Neel regions shown by the decrease of susceptibility dispersion, $\Delta\chi' = \chi_s - \chi_\infty$, from $\Delta\chi'|_{6.5\text{Oe}} = 0.046$ emu mL$^{-1}$ Oe$^{-1}$ to $\Delta\chi'|_{65\text{Oe}} = 0.033$ emu mL$^{-1}$ Oe$^{-1}$ (evaluated from Table II) was translated to be simply the result of the saturation of magnetic moments.

Meanwhile, $\chi''(\chi')$ plots of specimen 2 [Fig. 6(b)] show the presence of a skewed arc which was well fitted with the Cole-Davidson model. This asymmetric relaxation behavior, which analytically comes from the suppression of the phase delay

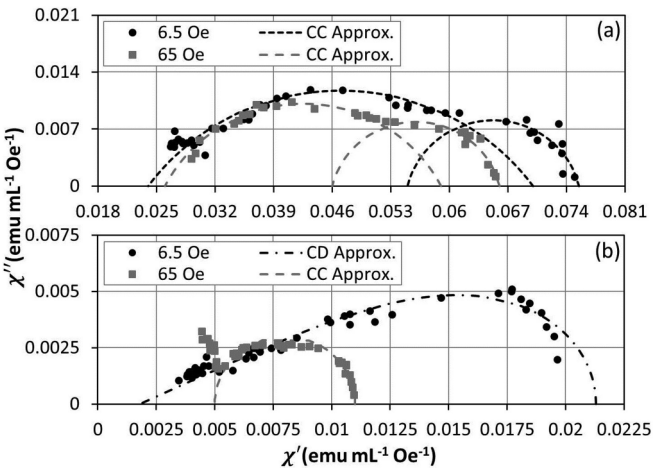


FIG. 6. Cole-Cole (CC) and Cole-Davidson (CD) graphical analyses of specimens show distinguishable relaxation regions. The respective plotting properties are shown in Table II. Plots of $\chi''(\chi')$-based experimental data at 6.5 Oe rms (black circles) are well fitted by the Cole-Cole model (black dashed line) for specimen 1 and by the Cole-Davidson model (black dash-dotted line) for specimen 2. Meanwhile, the $\chi''(\chi')$ plots of the experimental data at 65 Oe rms (gray squares) for both specimens are suitably fitted with the Cole-Cole model (gray dashed line).

TABLE II. Cole-Cole and Cole-Davidson plotting parameters.

| | | Brownian region | | | | Neel region | | |
|---|---|---|---|---|---|---|---|---|
| Specimen | $H$ (Oe) | $\alpha$ | $\beta$ | $\chi_s$ (emu mL$^{-1}$ Oe$^{-1}$) | $\chi_\infty$ (emu mL$^{-1}$ Oe$^{-1}$) | $\alpha$ | $\chi_s$ (emu mL$^{-1}$ Oe$^{-1}$) | $\chi_\infty$ (emu mL$^{-1}$ Oe$^{-1}$) |
| 1 | 6.5 | 0.15 | | 0.076 | 0.055 | 0.40 | 0.070 | 0.024 |
| | 65 | 0.15 | | 0.066 | 0.046 | 0.30 | 0.059 | 0.026 |
| 2 | 6.5 | | 0.28 | 0.021 | 0.0018 | | | |
| | 65 | 0 | 1 | 0.011 | 0.0050 | | | |

of the magnetization of individual particles to $\beta \tan^{-1} \omega\tau$, implies that another relaxation mechanism coexists with that of individual particles so that the additional friction forces from such possible cluster rotations may considerably decrease the absorption $\chi''$ in higher frequency. Using the Cole-Davidson plot, we could only confirm the initial Brownian relaxation region of specimen 2, which is confined by $\chi_s = 0.021$ emu mL$^{-1}$ Oe$^{-1}$ and $\chi_\infty = 0.0018$ emu mL$^{-1}$ Oe$^{-1}$. The nonlinear magnetization response of increasing magnetic field strength, which seems to induce a shorter Brownian relaxation time as confirmed in Fig. 4(b), can be associated with the change in $\Delta\chi'$ (from $\Delta\chi'|_{6.5\text{Oe}} = 0.019$ emu mL$^{-1}$ Oe$^{-1}$ to $\Delta\chi'|_{65\text{Oe}} = 0.0060$ emu mL$^{-1}$ Oe$^{-1}$) and the change in the maximum imaginary part of the magnetic susceptibility $\chi''_{\max}$ (from $\chi''_{\max}|_{6.5\text{Oe}} = 0.0048$ emu mL$^{-1}$ Oe$^{-1}$ to $\chi''_{\max}|_{65\text{Oe}} = 0.0028$ emu mL$^{-1}$ Oe$^{-1}$) of a left-shifted Brownian region. Furthermore, a semicircle-like curve of the $\chi''(\chi')$ plot associated with a single effective Brownian relaxation time was also observed at 65 Oe. This change in relaxation symmetry will be further discussed in relation to field-strength-dependent particle behavior.

## IV. DISCUSSION

### A. Physical model of relaxation

In sterically stabilized magnetic suspension (no sedimentation), the suspended particles (either dispersed or clustered) freely move as random Brownian motion in the absence of external magnetic fields. Once uniform alternating magnetic fields are introduced, the particles should be trapped within the fields and should show a limited movement. The relaxation responses of magnetization may appear in either particle or magnetic-moment rotation while the particles stay in their position; nonrotational Brownian motions (i.e., temperature-dependent particle diffusion) can be omitted in the case of dense suspensions [28]. If this condition is satisfied, adjacent particles with different sizes may create instant magnetic dipoles which affect the overall relaxation time of suspensions. Thus, we mainly treat Fig. 4 as being the result of dipolar interaction in addition to the polydispersity effect of either hydrodynamic size or particle size. In this paper, the contribution of Neel relaxation to relaxation dynamics will not be further discussed.

We found that the existence of Brownian relaxation greatly depends on the applied field strength in addition to temperature and frequency (Fig. 5). In the dispersed-particle system of specimen 1, applying a low sinusoidal magnetic field strength $H$ causes a particle rotation with a steady-state rotation angle related to the resultant of working torques [29]. Increasing the field strength may give rise to a larger rotation angle, but the presence of dipolar magnetism should confine the maximum allowable rotation angle. Unlike this system, the significance of dipolar magnetism in the case of the clustered-particle system of specimen 2, in which $N$ particles are encapsulated within a polymer shell, yielding a micelles-like structure, is much greater due to the smaller distance between particles; the dipolar interaction energy $E_d$ of a particle with magnetic moment $m$ at a distance $d$ from another particle is proportional to $d^{-3}$ [30,31]. The different viscosities of inner and outer clusters may also contribute to determining favorable physical relaxation [32,33]. Thus, exposing the system to low alternating magnetic field strength enables the cluster to rotate since particle rotations inside the clusters are highly limited by strong attractive interaction ($E_d \geqslant mH$) and higher inner friction, leading to strong enough overall magnetic torque to initiate a cluster rotation. However, its angle should also decrease at higher field strength since dipolar interactions are gradually broken ($E_d \ll mH$), resulting in stronger Brownian relaxation of individual particles inside the clusters. An illustration of these two different approaches to Brownian relaxation is shown in Fig. 7. We believe that the evolutional relaxation behavior of specimen 2 correlates to higher nonlinearity of its magnetization response compared to that of specimen 1.

### B. Change in hydrodynamic volume

The coexistence of two possible Brownian relaxation mechanisms, cluster rotation and individual particle rotation, leads to a field-strength-dependent change in its relaxation symmetry which can be generalized from Fig. 6(b). Individual magnetic torque $\sigma_{m,k}$ experienced by the $k$th composing particle seems to be a key point for describing such rotational relaxation dynamics of a clustered-particle system since the application of alternating magnetic field triggers different phase delays of magnetization $\varphi_k$ shown by individual particles within the cluster. In terms of Brownian relaxation, the resulting relaxation loss of specimen 2 induced by the applied sinusoidal magnetic field should be equal to total rotational friction losses owing to the principle of torque balance [22,34]. The total energy loss as a result of friction is composed of outer friction loss $E_{\text{CF}}^{\text{Out}}$ due to cluster rotation under outer viscosity $\eta_o$ and inner friction loss $E_{\text{CF}}^{\text{In}}$ caused by particle rotation under inner viscosity $\eta_i$, with different viscosities $\eta_o < \eta_i$. Thus, the energy balance can be written as Eq. (5), with further details

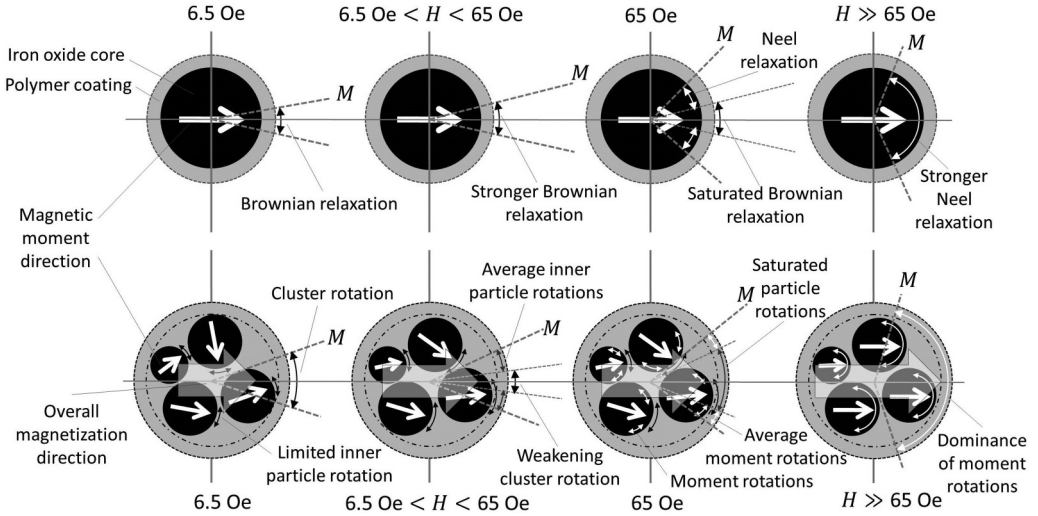


FIG. 7. Illustration of the field-strength-dependent relaxation dynamics of dispersed particles and clustered particles at low frequency and constant temperature describing the evolution of relaxation modes. Brownian relaxations (black two-headed arrows) are gradually replaced by Neel relaxation (white two-headed arrows) at higher field strength. In the case of a clustered-particle system, cluster friction should be less than individual particle friction to allow cluster rotation.

given in Eq. (6):

$$E_M - E_{\mathrm{CF}}^{\mathrm{In}} = E_{\mathrm{CF}}^{\mathrm{Out}}, \tag{5}$$

$$\sum_k \varphi_k V_{m,k}\sigma_{m,k} - \sum_k 6\eta_i V_{h,k}^m \omega\theta_{B_{p,k}}^{\max} = 6\eta_o V_h^c \omega\theta_{B_c}^{\max}. \tag{6}$$

Here, $V_{m,k}$, $V_{h,k}^m$, and $\theta_{B_{p,k}}^{\max}$ are the corresponding particle volume, rotatable volume, and maximum particle rotation angle of each particle, respectively, whereas $V_h^c$ and $\theta_{B_c}^{\max}$ are the initial hydrodynamic volume at low or zero field and the maximum rotation angle of the cluster.

The relaxation behavior of the clustered-particle system was suitably described by the Cole-Davidson model, in which the phase delay of magnetization corresponds to $\beta\varphi$. Thus, by defining a collective magnetic torque experienced by a cluster as $\bar{\sigma}_m$ so that $\sum_k \varphi_k V_{m,k}\sigma_{m,k} = \beta\varphi V_h\bar{\sigma}_m$, with $\bar{\sigma}_m \neq N\sigma_m$ and $\sigma_m = \sigma_{m,k}$, we found a correlation between the empirical $\beta$ parameter and the change in the hydrodynamic volume under high field strength due to the alteration of the rotation mode from cluster rotation to particle rotation. This finding is interpreted as the general behavior of particles inside the cluster. As estimated according to [35] from the Brownian peaks in Fig. 4(b) with constant viscosity and temperature ($\eta = 1$ cP, $T = 300$ K), the hydrodynamic volume $V_h$, however, changes from $V_h|_{6.5\mathrm{Oe}} = 2.3 \times 10^{-22}$ m$^3$ to $V_h|_{65\mathrm{Oe}} = 2.9 \times 10^{-23}$ m$^3$.

In agreement with the above rationalization, we experimentally confirmed the change in the $\beta$ parameter at higher field strength, which should be followed by the change in $\theta_{B_c}^{\max}$ since there is a constraint of $0 < \beta \leqslant 1$. This model states that the condition of $\beta = 1$ represents symmetric relaxation accounting for only particle rotation ($\theta_{B_c}^{\max} = 0$), while $0 < \beta < 1$ represents asymmetric relaxation accounting for the existence of either cluster rotation or particle rotation ($\theta_{B_c}^{\max} \neq 0$). We found that increasing the field strength from 6.5 to 65 Oe changes the $\beta$ parameter from $\beta|_{6.5\mathrm{Oe}} = 0.28$ to $\beta|_{65\mathrm{Oe}} = 1$. Hence, this change in the $\beta$ parameter proves that the change in the hydrodynamic volume of physical rotation occurs, causing the effective Brownian relaxation to shift to higher frequency. We also underline that the field-strength-dependent $\beta$ parameter not only is a fitting parameter of the empirical relaxation model but also represents how significant the interparticle interaction is and further points out how the energy dissipates microscopically in a clustered-particle system.

## V. CONCLUSION

We performed an experimental study of relaxation behaviors in superparamagnetic iron oxide nanoparticle suspensions by measuring multivariable-dependent complex magnetic susceptibility. We observed a decrease in the real part of the magnetic susceptibility at higher field strength in addition to the broadening distribution of the imaginary part against frequency. In terms of temperature dependence, this nonlinear magnetization found at low frequency was mostly due to Brownian relaxation in which the significance of the interparticle interaction in each specimen could be associated with the degree of nonlinearity. We came to the conclusion that the coexistence of cluster rotation and individual particle rotations in the clustered-particle system gives rise to field-strength-dependent relaxation symmetry. It was found that the application of low field strength results in the dominance of cluster rotation due to strong dipolar interactions between individual particles. More interestingly, the change in the Brownian relaxation behavior associated with a shorter relaxation time occurred at higher field strength, suggesting a smaller hydrodynamic volume. This change from cluster rotation to individual particle rotations could be empirically attributed to the change in the $\beta$ parameter of the Cole-Davidson analysis of the non-Debye relaxation model which constitutes the significance of interparticle interactions. We considered this distinguishable Brownian relaxation dynamics to be one of the origins of the highly nonlinear response of magnetization in the clustered-particle system.

[1] H. Mamiya and B. Jayadevan, Sci. Rep. **1**, 157 (2011).
[2] J. Lampe, C. Bassoy, J. Rahmer, J. Weizenecker, H. Voss, B. Gleich, and J. Borgert, Phys. Med. Biol. **57**, 1113 (2012).
[3] T. Fuchigami, R. Kawamura, Y. Kitamoto, M. Nakagawa, and Y. Namiki, Biomaterials **33**, 1682 (2012).
[4] A. V. Orlov, J. A. Khodakova, M. P. Nikitin, A. O. Shepelyakovskaya, F. A. Brovko, A. G. Laman, E. V. Grishin, and P. I. Nikitin, Anal. Chem. **85**, 1154 (2013).
[5] R. E. Rosensweig, J. Magn. Magn. Mater. **252**, 370 (2002).
[6] S. Biederer, T. Knopp, T. F. Sattel, H. K. Lüdtke-Buzug, B. Gleich, J. Weizenekcer, J. Borgert, and T. M. Buzug, J. Phys. D **42**, 205007 (2009).
[7] A. K. Bhuiya, T. Mitake, M. Asai, T. Ito, S. Chosakabe, T. Yoshida, K. Enpuku, and A. Kandori, IEEE Trans. Magn. **47**, 2867 (2011).
[8] D. Ling and T. Hyeon, Small **9**, 1450 (2013).
[9] W. F. Brown, J. Appl. Phys. **34**, 1319 (1963).
[10] L. Néel, Ann. Geophys. **5**, 99 (1949).
[11] R. Hergt, S. Dutz, R. Müller, and M. Zeisberger, J. Phys. Condens. Matter **18**, S2919 (2006).
[12] R. M. Ferguson, K. R. Minard, A. P. Khandhar, and K. M. Krishnan, Med. Phys. **38**, 1619 (2011).
[13] S. H. Chung, A. Hoffmann, S. D. Bader, C. Liu, B. Kay, L. Makowski, and L. Chen, Appl. Phys. Lett. **85**, 2971 (2004).
[14] X. Z. Cheng, M. B. A. Jalil, H. K. Lee, and Y. Okabe, J. Appl. Phys. **99**, 08B901 (2006).
[15] V. Signh, V. Banarjee, and M. Sharma, J. Phys. D **42**, 245066 (2009).
[16] N. A. Usov and B. Y. Liubimov, J. Appl. Phys. **112**, 023901 (2012).
[17] T. Yoshida, K. Enpuku, J. Dieckhoff, M. Schilling, and F. Ludwig, J. Appl. Phys **111**, 053901 (2012).
[18] D. Eberbeck, F. Wiekhorst, U. Steinhoff, and L. Trahms, J. Phys. Condens. Matter **18**, S2829 (2006).
[19] C. Ravikumar, S. Kumar, and R. Bandyopadhyaya, Colloids Surf. A **403**, 1 (2012).
[20] W. Wu, Q. He, and C. Jiang, Nanoscale Res. Lett. **3**, 397 (2008).
[21] L. Zhang, R. He, and H.-C. Gu, Appl. Surf. Sci. **253**, 2611 (2006).
[22] M. I. Shliomis, Sov. Phys. Usp. **17**, 153 (1974).
[23] G. Wang and J. P. Huang, Chem. Phys. Lett. **421**, 544 (2006).
[24] K. Nakamura, K. Ueda, A. Tomitaka, T. Yamada, and Y. Takemura, IEEE Trans. Magn. **49**, 240 (2013).
[25] K. S. Cole and R. H. Cole, J. Chem. Phys. **9**, 341 (1941).
[26] D. W. Davidson and R. H. Cole, J. Chem. Phys. **19**, 1484 (1951).
[27] Y. Onodera, J. Phys. Soc. Jpn. **62**, 4104 (1993).
[28] M. A. Islam, Phys. Scr. **70**, 120 (2004).
[29] D. B. Reeves and J. B. Weaver, J. Appl. Phys. **112**, 124311 (2012).
[30] M. F. Hansen and S. Mørup, J. Magn. Magn. Mater. **184**, L262 (1998).
[31] S. Mørup, M. F. Hansen, and C. Frandsen, Beilstein J. Nanotechnol. **1**, 182 (2010).
[32] R. Kötitz, P. Fannin, and L. Trahms, J. Magn. Magn. Mater. **149**, 42 (1995).
[33] B. Fischer, B. Huke, M. Lücke, and R. Hempelmann, J. Magn. Magn. Mater. **289**, 74 (2005).
[34] M. I. Shliomis and V. I. Stepanov, J. Magn. Magn. Mater. **122**, 196 (1993).
[35] T. Yoshida and K. Enpuku, Jpn. J. Appl. Phys. **48**, 127002 (2009).